JOURNAL OF CATALYSIS 145, 107–125 (1994)

Fluoride and Sulfate Treatment of $AlPO_4$–Al_2O_3 Catalysts

I. Structure, Texture, Surface Acidity, and Catalytic Performance in Cyclohexene Conversion and Cumene Cracking

F. M. Bautista,* J. M. Campelo,*,[1] A. Garcia,* D. Luna,* J. M. Marinas,* A. A. Romero,* J. A. Navio,† and M. Macias†

*Departamento Química Orgánica, Universidad de Córdoba, Avenida San Alberto Magno, s/n°, E-14004 Cordoba, Spain; and †Instituto Ciencia de Materiales, Universidad de Sevilla-CSIC/Departamento Química Inorgánica, Facultad de Química, E-41012 Seville, Spain

Received January 4, 1993; revised July 26, 1993

Anion-treated (APAl–P–F) and APAl–P–S) catalysts contain both tetrahedral and octahedral Al (their ratio varies with anion type), while P always remains in $P(OAl)_4$ environments. Moreover, two types of Al surface OH groups at 3786 and 3738 cm^{-1} and only one type of P surface OH group at 3670 cm^{-1} are found in the DRIFT spectra of the APAl–P catalyst. All OH types are reduced by anion treatment, especially in the case of the F^- ion (APAl–P–F). However, all catalysts retain some hydroxyl groups after anion treatment. The presence of F^- or SO_4^{2-} ions increases both the number and strength of acid sites and so all anion-modified APAl–P catalysts exhibited increased catalytic activity with respect to the unmodified ones in cyclohexene and cumene transformations. Also, each reaction responded in a similar way to anion modification. Moreover, APAl–P–F catalysts have increased activity as compared to the sulfated ones in both reaction processes. The maximum catalytic activity of APAl–P–F catalysts was observed when the fluoride loading was 2.5 wt%. In cyclohexene conversion, the anion type also causes a change in the reaction process. Thus, pure APAl–P and APAl–P–S catalysts are selective for cyclohexene isomerization while APAl–P–F catalysts exhibit both isomerization and hydrogen transfer activities, the former always being predominant. Maximum selectivity towards cyclohexene isomerization products is obtained at lower conversion, while the selectivity towards hydrogen transfer products (methylcyclopentane plus cyclohexane) increases with the fluoride content and reaction temperature.

INTRODUCTION

The effect of fluoride or sulfate incorporation on metal oxide catalysts has attracted much attention in recent years. Thus, it is known that the fluorination of Al_2O_3 or other metal oxides improves the activity of these catalysts for acid-catalyzed reactions (1–6). A maximum in catalytic activity is usually observed for catalysts with F^- concentrations between 1 and 10 wt%. Moreover, fluorination can cause changes in the selectivity of the catalysts for a given product as well as a significant reduction in coke formation during cracking reactions. The improvement in activity is associated with a change in the surface chemistry of the catalyst due to that, at low fluoride loading, surface oxide and hydroxyl groups are replaced by F^- ions (starting with the weakest protonic groups) which, because of the slightly higher electronegativity of fluorine, may polarize the lattice more than the groups replaced. This weakens the O–H bond and therefore enhances the acid strength of the remaining hidroxyl groups. The strength of Lewis sites is also enhanced by the incorporation of fluorine due to the inductive effect. The F^- ion also changes the activity of each acid site. At the same time, the small amount of F^- ion enhances electron-acceptor properties. These effects depend upon the nature of fluoride treatment, fluoride amount and further calcination. At higher fluorine content, other phases such as AlF_3 or AlF_2OH are formed (3).

On the other hand, several metal oxides containing SO_4^{2-} ions present strong surface acidity, and are increasingly used as solid acid catalysts (7–12). Besides, it is generally believed that this high acidity originates from the formation of a surface sulfur complex with a covalent S=O bond (bridging bidentate sulfate coordinated to metal elements). The double bond nature of the complex is much stronger than that of a simple metal sulfate and thus, its electronic induction effect enhances the Lewis acidity of the metal cation remarkably (7, 8, 10). If water molecules are present, Lewis acid sites are converted into Brønsted acid sites. SO_4^{2-} ions deposited on the oxides are known to be stable when calcined at 773 K. They remain on the surface even in the presence of hydrogen at 720 K although the sulfur is reversibly reduced from S^{6+} to S^{2-} (7).

[1] To whom correspondence should be addressed.

0021-9517/94 $5.00

In this context, post synthesis modification of $AlPO_4$ with F^- (13) or SO_4^{2-} (14, 15) ions causes changes in the porous texture and thermal stability, and in the concentration of acid and basic catalyst sites. Also, we have shown that cyclohexene skeletal isomerization can be enhanced by loading the catalyst with small amounts of F^- (13) or SO_4^{2-} (14, 15) ions and that, in the latter case, the modification leads to a greater increase than in the former. Besides, a high amount of anion (5 wt%) adversely affected the $AlPO_4$ structure and thus, crystallization of $AlPO_4$ occurred which resulted in a decrease in activity. Moreover, the addition of Al_2O_3 to $AlPO_4$ is very effective on increasing the catalyst performance for carbenium ion reactions (16, 17). So, our investigation is concerned with the modification of the catalytic performance of the $AlPO_4$–Al_2O_3 (25 wt% Al_2O_3) catalyst, obtained in propylene oxide, arising through the introduction of small amounts (1–3 wt%) of F^- or SO_4^{2-} ions.

In this work, the characterization of a series of ion-modified (1–3 wt% F^- or SO_4^{2-}) $AlPO_4$–Al_2O_3 catalysts was performed using XRD, TG-DTA, XPS, TPD of water, DRIFT, SEM, and N_2 adsorption. The surface acid properties were measured, at temperatures close to those employed in catalytic processes (473–673 K), through the chemisorption of pyridine (PY) and 2,6-dimethylpyridine (DMPY). Two model acid-catalyzed reactions are also studied to further characterize their acidic properties: cyclohexene and cumene conversions. In this sense, model reactions have been recommended (18) as the best method for characterizing industrial acid catalysts.

Also, cyclohexene was chosen as a test molecule since, while difficult to crack, it allows a rapid evaluation of the skeletal isomerization and hydrogen transfer tendency of the catalysts, i.e., formation of methylcyclopentenes or cyclohexane and methylcyclopentane (18–21). Besides, Parmaliana *et al.* (20) indicates that cyclohexene can be considered as a most reliable probe molecule for a number of catalytic functions: isomerization, hydrogen activation and hydrogen transfer.

Furthermore, cumene cracking was also studied since it is normally employed as standard test for the characterization of catalysts and for studying protonic acid sites on solid catalysts (22–24). Apparently, the Lewis acid sites alone are not active; however, Lewis acid sites in the vicinity of protonic sites can increase their strength and consequently their activity (25).

EXPERIMENTAL

Catalysts

$AlPO_4$–Al_2O_3 (APAl–P, 25 wt% Al_2O_3) was obtained in the presence of propylene oxide and calcined at 923 K for 3 h (16).

Fluorinated APAl–P catalysts (APAl–P–F) were prepared by impregnation until incipient wetness using an aqueous ammonium fluoride solution. After soaking the catalyst in this solution for 1 h, the impregnated APAl–P catalyst was dried at 393 K for 24 h and then calcined at 773 K for 3 h. An unmodified $AlPO_4$–Al_2O_3 (APAl–P–0) was prepared by placing it in water containing no fluoride ion, drying at 393 K for 24 h, and later on calcining at 773 K for 3 h.

The incorporation of SO_4^{2-} ions (APAl–P–S catalysts) was carried out by the same procedure used for APAl–P–F catalysts but using ammonium sulfate aqueous solution. In both cases the loading was in the range 1–3 wt%.

From catalytic studies obtained with the above catalysts, a new APAl–P–FM catalyst (2.5 wt% F^-) was prepared by impregnation using a methanolic (12.3 wt% H_2O) ammonium fluoride solution. Also a new unmodified APAl–P–0M catalyst was prepared. In both cases, thermal treatments were equal to the above described.

Values for the percentage of ions on the calcined APAl–P catalyst are based on the impregnated anion, assuming no loss of ion during calcination at 773 K. Other authors have reported no appreciable loss of anions during calcination (6, 26).

X-Ray Diffraction Measurements

XRD patterns were carried out with Ni-filtered CuK_α radiation (λ = 1.5418 Å). Samples were scanned at a speed of 2° min^{-1} (2θ = 10 to 60°) using a Siemens D-500 diffractometer (35 kV, 20 mA).

TGA and DTA Measurements

Thermogravimetric and differential thermal analyses were carried out in the presence of static air and a heating rate of 10 K min^{-1} (temperature range: 293–1550 K). The samples used were dried precipitates (393 K, 24 h) previous to calcination.

TPD/MS Measurements

The analysis of the evolved water produced and/or desorbing during sample heating was performed using temperature-programmed desorption, under helium flux (100 mL min^{-1}), by attaching the sample tube to a Faraday-cup detector; a heating rate of 5 K min^{-1} was used. The samples used for TPD/MS measurements were calcinated samples.

XPS Measurements

The XPS spectra were recorded on a Leybold-Heraeus LHS-10 spectrometer working with a pass energy constant of 50 eV and using AlK_α radiation ($h\nu$ = 1686.6 eV) as the excitation source. The spectra were submitted

to background subtraction and to area calculations. Binding energy values were referred to as C(1*s*) peak (pollution carbon) at 284.6 eV.

Scanning Electron Microscopy (SEM)

SEM studies were carried out in an ISI apparatus, model SS40, and the dispersion energy of X rays was measured by a KEVEX analyzer Model 8000; a semiautomatic image analyzer of magnetostrictive board KONTRON MOP-30 was used to estimate the weight average size of aggregates and particles.

NMR Spectroscopy Measurements

^{27}Al and ^{31}P MAS spectra were recorded at 104.26 and 161.98 MHz, respectively, with a Bruker ACP-400 spectrophotometer (external magnetic field, 9.4 T). Measurements were carried out at room temperature with spinning in the 5–5.5 kHz range. ^{31}P spectra were recorded after $\pi/2$ pulse excitation (2.6 μs) and the intervals between successive accumulations (6 s) were chosen to avoid saturation effects. ^{27}Al spectra were obtained after a 2-μs pulse ($\pi/4$ pulse) and a recycling time of 2 s. $NaH_2PO_4 \cdot 2H_2O$ and $Al(H_2O)_6^{3+}$ solutions were used as external standard references for P and Al chemical shifts, respectively. To preserve quantitative analysis, no mathematical procedures of NMR signal treatment, such as multiplication by an exponential function, were used. Also, the chemical shifts given for Al were not corrected for second-order quadrupole effects.

Textural Properties

Specific surface areas of anion-treated APAl–P catalysts were obtained from the analysis of the nitrogen adsorption–desorption isotherms by using the BET procedure. The reproducibility of most isotherms was checked.

DRIFT Measurements

Diffuse reflectance FTIR (DRIFT) spectra were recorded on a FTIR instrument (Bomem MB-100) equipped with an "environmental chamber" (Spectra Tech, P/N 0030-100) placed into a diffuse reflectance attachment (Spectra Tech, Collector). A resolution of 8 cm^{-1} was used with 256 scans being averaged to obtain spectrum from 4000 to 400 cm^{-1}. Single-beam spectra were ratioed against KBr or APAl–P–0 reference spectra collected at the same temperature as the sample. In the latter mode of presentation the downward bands are due to decreased species (in the progress of the anion treatment) and the upward bands are attributable to the formed species. A plot of pseudo-absorbance has been preferred. This allowed direct subtraction of spectra obtained with the same sample under different conditions. The temperature controller was calibrated to the actual sample temperature by inserting a thermocouple directly into a sample and monitoring the sample temperature at different controller settings. The samples were diluted to 15 wt% in KBr.

DRIFT spectra have been recorded for all the calcinated catalysts previously dried at 400 K for 24 h under vacuum. Afterwards, the catalyst was placed in the environmental chamber cell with a 20 ml min^{-1} flow of dehydrated and deoxygenated nitrogen, heated to 573 K and held at this temperature for 1 h prior to carrying out the spectrum. Higher nitrogen flushing times or vacuum treatment do not modify the DRIFT spectra. In some cases, spectra of the O–H stretching region were smoothed with a five-point Savitzky–Golay algorithm.

In DRIFT characterization of surface acidity, PY and DMPY were introduced by bubbling a stream of dehydrated and deoxygenated nitrogen (20 ml min^{-1}) through the liquid and into the sample chamber containing the neat (no KBr diluted) catalyst sample at 373 K. Samples were equilibrated for at least 1 h at each temperature (373, 473, and 573 K) or reactant condition prior to collection of spectra. Excess reactant was evacuated from the sample chamber.

Surface Acidity Measurements

The surface acidity (sum of Brønsted and Lewis sites) was measured in a dynamic mode by means of the gas-phase (473–673 K) adsorption of PY and DMPY using a pulse-chromatographic technique (27) according to a method described elsewhere (28). Very small volumes of solutes were injected so as to approach conditions of gas-chromatography linearity. The acidity measurements were repeated several times and good reproducibility of the results was obtained.

Catalytic Measurements

The catalytic measurements were carried out in a microcatalytic pulse reactor according to a method previously described (29, 30) and under the following conditions.

(*a*) *Cyclohexene conversion.* hydrocarbon pulse, 1 μl; temperature, 523–673 K (at 50 K intervals); carrier gas, nitrogen (40 ml min^{-1}). GC with FID and two columns ($\frac{1}{8}$", stainless-steel, 2 m each) in series packed with, respectively, 5% polyphenylether (6-rings) and 5% squalane both on Chromosorb G AW-DMCS 80/100 at 323 K.

(*b*) *Cumene conversion.* hydrocarbon pulse, 1 μl; temperature, 573–773 K (at 50 K intervals); carrier gas, nitrogen (20 ml min^{-1}). GC with FID and a 2-m column ($\frac{1}{8}$" stainless-steel) packed with 5% polyphenylether (6-rings) on Chromosorb G AW-DMCS 80/100 at 373 K.

In separate experiments, both reactions were carried out by using the split–splitless capillary injection system

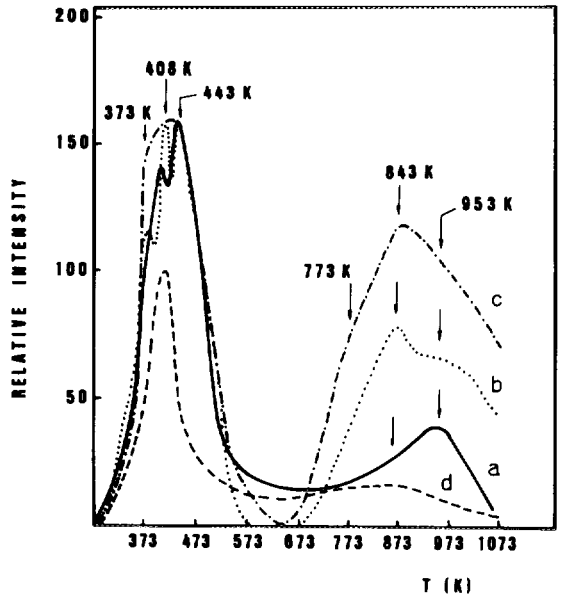

FIG. 1. Temperature-programmed desorption profiles of H_2O desorbing from the studied catalyst surfaces: (a) APAl–P–0, (b) APAl–P–2.5S, (c) APAl–P–2.5F, and (d) γ-Al_2O_3 (as reference).

of a Hewlett–Packard 5890 II gas-chromatograph as the microcatalytic pulse reactor in order to characterize the reaction products by GC–MS (HP 5970 MSD quadrupole mass spectrometer). The reaction products, analyzed using a 60-m SPB-1 capillary column (Supelco) at 308 K, were 1- and 3-methylcyclopentenes (1- and 3-MCPE), methylcyclopentane (MCPA), and minor amounts of cyclohexane (CHA), for cyclohexene conversion, and propylene, benzene (BZ), and α-methylstyrene (MS) for cumene cracking.

Cyclohexene and cumene (from Merck) were used after distillation and purification with a column of alumina previously calcined at 573 for 3 h.

RESULTS AND DISCUSSION

DTA Measurements and XRD Studies

All anion-modified APAl–P catalysts are amorphous and remain amorphous after the catalytic reactions.

TPD/MS Experiments

The TPD profiles of water desorbing from γ-Al_2O_3 and unmodified and anion loaded (2.5 wt%) APAl–P catalysts, are shown in Fig. 1.

Below 623 K, the TPD profiles for APAl–P–0 and anion loaded catalysts are rather similar with molecular water desorbing at about 373, 408, and 443 K and with different relative peak intensities of water desorbing at the same temperature which shown different intensity values from one sample to another; these peaks could reflect different types of adsorbed molecular water. However, for γ-Al_2O_3 our TPD results showed that the molecular water seemed to desorb mainly in one definite state centered at about 408 K, therefore indicating a certain degree of homogeneity in site distributions. The differences in the shape of TPD profiles between the APAl–P samples and γ-Al_2O_3 could be explained in terms of the effect of phosphate and either fluoride or sulfate anions, leading to different types of heterogeneous site distributions.

Results from Fig. 1 showed that unmodified and anion-treated APAl–P catalysts also exhibited water desorption peaks centered at 773, 843, and 953 K. As can be observed, the water desorption over 623 K is more accentuated for the anion-treated APAl–P catalysts (especially in the APAl–P–F case) than that for the APAl–P–0 sample. These results indicate that after incorporation of either F^- or SO_4^{2-} ions, a certain number of strongly adsorbed hydroxyl groups developed which seemed to desorb in the temperature range between 623 and 1000 K. This kind of water desorbed can arise from the polycondensation of acidic hydroxyl groups, possibly species H^+ slightly linked to $O^=$ anions with a certain degree of mobility at the surface ($O^=$ . . . . . H^+). In this sense Yang *et al.* (31) reports the appearance of a desorption peak at temperatures over 673 K (during the TPD of ammonia adsorbed on alumina–aluminum phosphate) due to surface dehydration.

XPS Results

The elemental surface composition of APAl–P–0, APAl–P–2.5F, and APAl–P–2.5S catalysts is collected in Table 1. As can be seen from Table 1, the surface concentration ratio $[P]_s/[Al]_s$ of anion-treated samples is practically the same as the unmodified one. Moreover, the ratios of oxygen to aluminum (=3.61) and oxygen to phosphorus (=6.11) for the APAl–P–0 catalyst exceeded the expected values of stoichiometric composition. This may be due to the presence of hydroxyl groups linked to P or Al atoms.

TABLE 1

Elemental Surface Composition and XPS Binding Energies[a] of the Elements Present at the Surface of Unmodified and Anion-Treated APAl–P Catalysts Calcined at 773 K for 3 h

Catalyst	Surface concentration (at%)					
	P (2p)	Al (2p)	O (1s)	C	F (1s)	S (2p)
APAl–P–0	11.4(134.2)	17.1(74.8)	62.0(532.0)	9.4	—	—
APAl–P–2.5F	12.5(133.5)	18.8(74.1)	65.6(531.4)	—	3.0(684.9)	—
APAl–P–2.5S	11.6(133.6)	17.8(74.1)	65.7(531.4)	4.3	—	0.6(168.9)

[a] In parenthesis, eV.

Besides, the various core lines investigated for different samples were very similar and all appeared as single symmetrical lines, indicating a homogeneous distribution of the electron densities around the atoms throughout the solid. Table 1 also collects the XPS binding energies (eV) of elements present on the surface of catalysts. All values were referenced to the C(1*s*) peak at 284.6 eV.

From Table 1 it is evident that, in APAl–P–2.5S catalyst, XPS investigations gave a S(2*p*) signal at the binding energy of 168.6 eV attributed to S^{6+} therefore suggesting that the oxidation state of sulfur as SO_4^{2-} is the main species. Besides, we can also notice that the fluorination of APAl–P catalyst does not cause relevant chemical shifts in the Al(2*p*) signal. Thus, the possible formation of surface AlOF and AlF3 components should be discarded.

Furthermore, note that in the APAl–P–0 sample, an O(1*s*) peak is observed at a binding energy of 532.0 eV, typical of OH surface species, which is indicative of a slight hydroxylation of this material. However, after fluoride or sulfate addition, the O(1*s*) peak is slightly displaced toward lower binding energy (531.4 eV) which could be associated with the surface oxygen atom, although the presence of surface hydroxyl groups could also be responsible for this signal since the O(1*s*) peak of Al_2O_3 is currently observed at 531.8 eV and is also assigned to the OH surface species (32).

SEM Studies

SEM results of APAl–P–0, APAl–P–2.5F, and APAl–P–2.5S catalysts are shown in Fig. 2.

SEM observation showed a very unhomogeneous distribution in morphology and particle sizes. The average size of the particles was around 45 μm. A microanalysis at the surface of the particles (EDX) showed a very homogeneous distribution of P and Al, not only in the particles but also between the particles.

In APAl–P–2.5S catalyst we observe a greater tendency to the formation of spherical deposits with respect to the APAl–P–2.5F one. This could be due to a large SO_4^{2-} catalyst interaction.

NMR Spectroscopy

Figure 3 shows the ^{27}Al MAS spectrum of APAl–P–0, APAl–P–2.5F, and APAl–P–2.5S catalysts. The spectra contains a broad peak at 40 ppm, typical of tetrahedral aluminum sharing oxygens with four tetrahedra of phosphorus [$Al(OP)_4$], and a small one at $\simeq -6$ ppm, characteristic of octahedrally coordinated Al sites, Al(VI) (33, 34).

The ^{31}P MAS spectra (Fig. 3) showed a broad line at $\simeq -23$ ppm. This chemical shift corresponded to P atoms in tetrahedral coordination with P–O–Al bonds (i.e., $P(OAl)_4$ environments). It appears that the chemical shifts of P in different sites are similar, resulting in a broadened peak.

The amount of Al(VI) decreased with fluoride loading while SO_4^{2-} ions scarcely affected the Al(IV)/Al(VI) relation. However, the position of the ^{27}Al and ^{31}P remained almost unchanged. So, the ion incorporation did not change the local structure of the starting catalyst; the spectra of samples was very similar to those obtained for APAl–P–0 sample. These data indicated that F^- ion substitutes for OH groups in aluminum octahedra supported the mechanism suggested by Gerberich *et al.* (6) that established the formation of isolated Al–F species in slightly fluorinated aluminas. So, fluorination of Al-PO_4-Al_2O_3 catalysts resulted in a decreased concentration of hydroxyl groups (see DRIFT measurements).

Textural Properties

Nitrogen isotherms were type IV exhibiting hysteresis loops (type H1) at the higher pressure range and hence, corresponding to the presence of mesopores in the samples (35). The *n*-plots (36) also strengthen these facts and, besides, the surface areas calculated by the *n*-method (S_n) were found to tally with those obtained by the BET method, S_{BET}, as shown in Table 2. Furthermore, *n*-plots also indicates that the samples are free of micropores. Table 2 also includes the mean pore radius ($r = 2V_P/S_{BET}$) of the samples.

The results in Table 2 show that after sulfate incorporation, the surface area decreases slightly (possibly due to the plugging of small pores by impregnation) while the pore volume remains almost unchanged. Furthermore, the main pore radius increases slightly according to a progressive coalescence of pores parallel to the drop in the surface area. Thus, in APAl–P–S catalysts the trend of high surface area still exists.

Besides, as shown in Table 2, the incorporation of F^- ion into APAl–P–0 catalyst leads, simultaneously, to a strong decrease in surface area and pore volume and an increase in the most frequently occurring pore radius. The decrease in surface area after fluorination is frequent and depends on the fluorine content and fluorination process (3, 26).

DRIFT Spectra of Catalysts

The DRIFT spectra (OH stretching vibration region) of APAl–P–0, APAl–P–2.5F, and APAl–P–2.5S catalysts (Fig. 4A) show bands of surface Al–OH (with Al atoms in tetrahedral coordination) at 3786 cm^{-1} and of unbonded surface P–OH at 3674 cm^{-1}. A shoulder at $\simeq$3739 cm^{-1} is also found. This is due to stretching vibrations of surface Al–OH with Al atoms in octahedral coordination (37).

Also, a very broad band at $\simeq$3580 cm^{-1} is found. This band is due to surface hydroxyl groups, most likely phos-

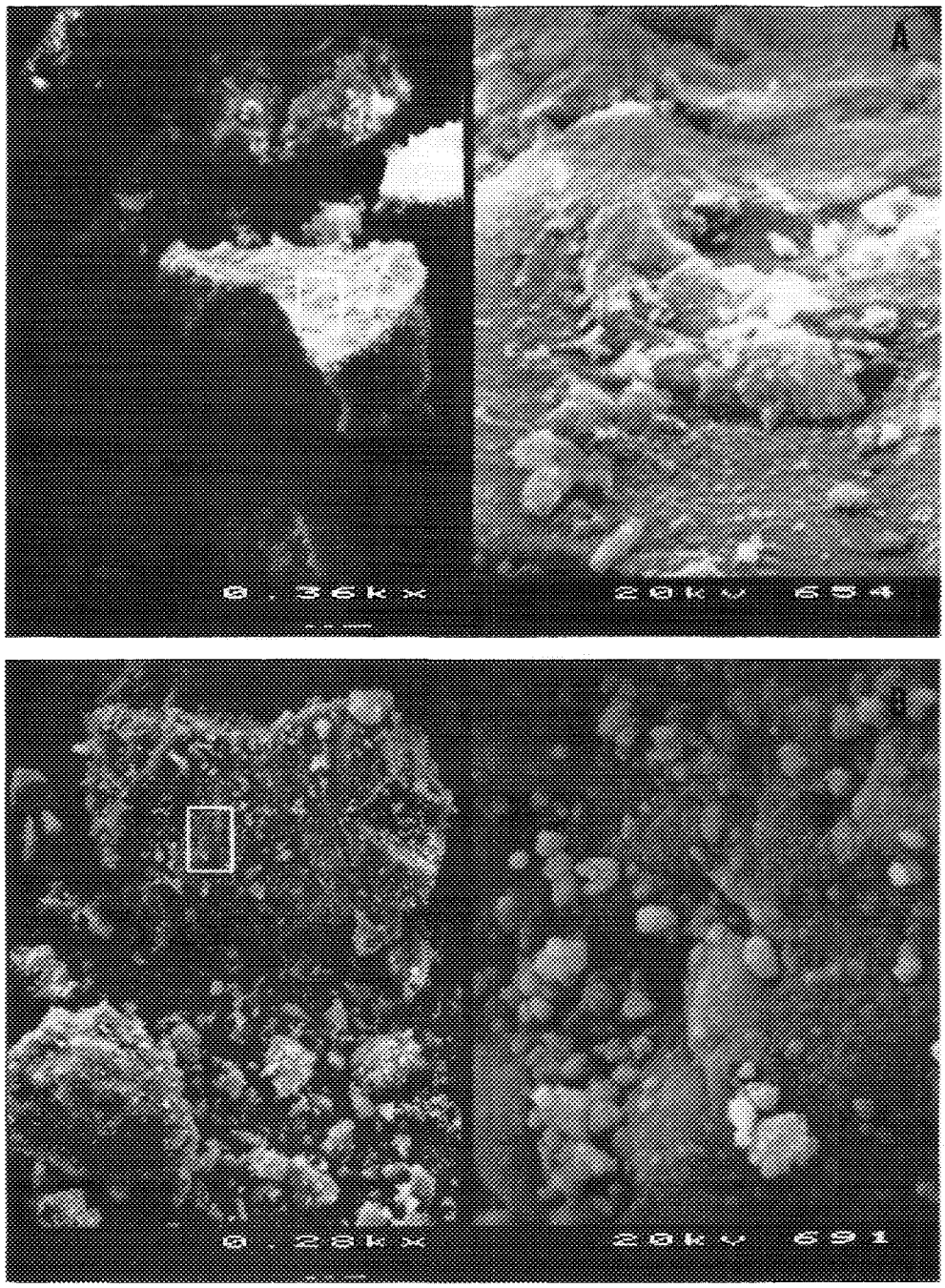

FIG. 2. SEM micrographs: (a) APAl–P–0; (b) APAl–P–2.5F, (c) APAl–P–2.5S.

phorus ones, perturbed by a hydrogen bridge bond from a surface hydroxyl band. Besides, in anion-modified catalysts we can observe a shoulder around 3300 cm^{-1} that is more accentuated in fluorided APAl–P samples. This band may be associated with acidic OH_a^- ($O^= \ldots H^+$) groups. However, this shoulder is absent in the APAl–P–0 sample.

As can be seen from Fig. 4B, after the F^- ion was loaded in the APAl–P sample, the bands at 3786, 3739, and 3674 cm^{-1}, due to O–H stretching vibrations, decreased in intensity as compared to the APAl–P–0 catalyst (in this representation mode, the downward bands are due to decreased species in the progress of fluoridation). This indicated that the F^- ion substitutes for both Al–OH and P–OH groups in the APAl–P–0 catalyst. Moreover, as fluoride loading increases OH stretching vibration bands smoothly increase in intensity (more negative) indicating a more developed OH substi-

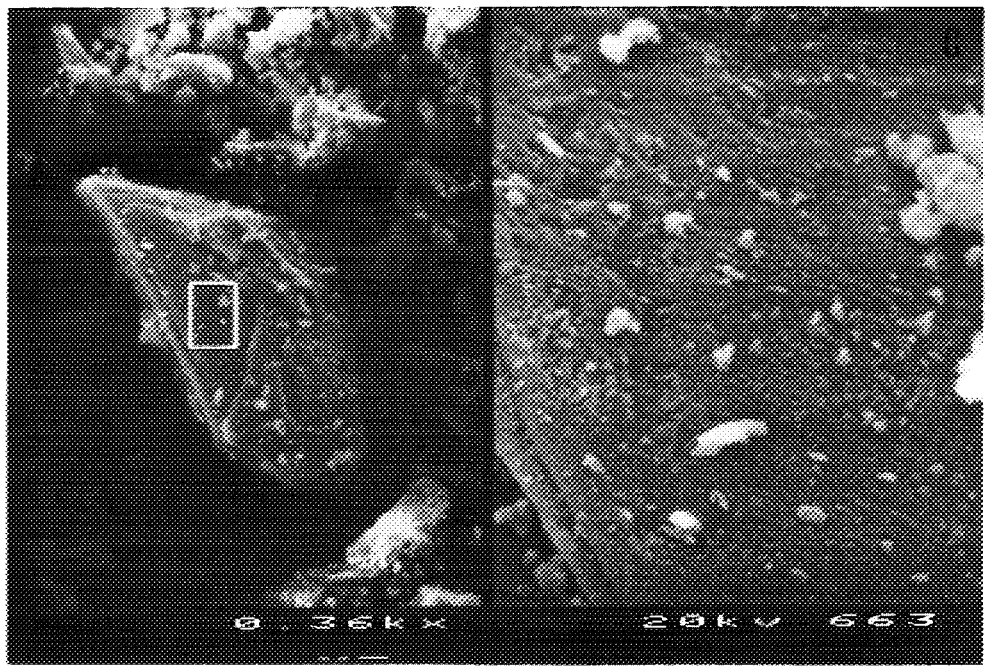

FIG. 2—*Continued*

tution by the fluoride ion. However, some of the hydroxyl groups are still present at 3 wt% F; these remaining OH groups ought to be the strong protonic centres that are enough able to protonate 2,6-dimethylpyridine (see below).

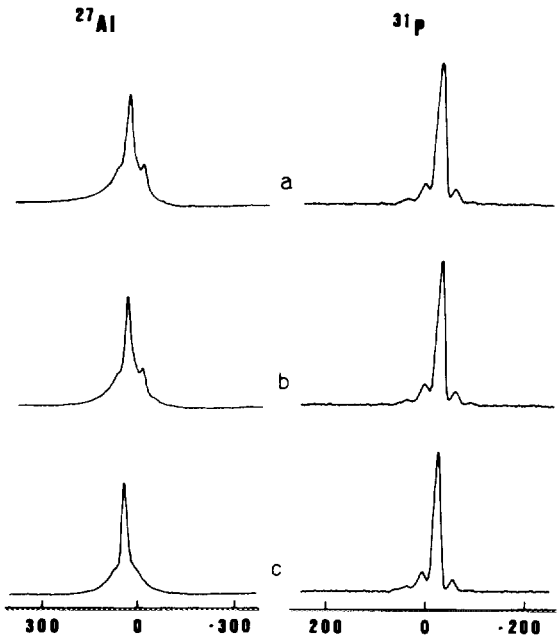

FIG. 3. ^{27}Al (104.26 MHz) and ^{31}P (161.98 MHz) MAS-NMR spectra of catalysts calcined at 773 K for 3 h: (a) APAl–P–0; (b) APAl–P–2.5S; and (c) APAl–P–2.5F.

Moreover, APAl–P–S catalysts also exhibit a decrease in the intensity of Al–OH and P–OH bands, although dehydroxylation is less accentuated (results not shown). The remaining surface OH groups also protonate 2,6-dimethylpyridine (see below).

Furthermore, in Fig. 5a the spectrum of the surface sulfate species (1800–600 cm^{-1} region) on APAl–P–3S is shown. Drastic spectral changes are seen in that region and the bands can be assigned to sulfate species because of their positions and the lack of these bands in other samples which do not contain sulfate.

The APAl–P–3S sample gave an upward band at 1308 cm^{-1} with a shoulder at $\simeq$1385 cm^{-1} after treatment in nitrogen (20 ml min^{-1}) at 573 K for 1 h (Fig. 5a). These bands exhibited low intensity as corresponded to the low sulfate content and to the moderately high surface area of the sample. Bands in this region have been attributed to S–O vibrations of surface groups (7, 8, 38–41). Thus, the band at $\simeq$1385 cm^{-1} can be assigned to the asymmetric stretching vibration of the S=O bonds where the sulfur atom would be in a pseudotetrahedral coordination with four oxygen atoms forming a bidentate sulfate ion. In this sense, XPS investigations (see above) of the APAl–P–3S catalyst gave the signal attributed to S^{6+} (binding energy, BE = 168.6 eV), suggesting that the oxidation state of sulfur as SO_4^{2-} was the main species.

The band at 1308 cm^{-1} is also a characteristic of the S=O group (7, 41) and has been related with association with H_2O or with surface hydroxyls (7, 38). However, so far the real structure of the active sites responsible for

TABLE 2

Textural Properties and Surface Acidity of APAl–P Catalyst Containing Fluoride and Sulfate Ions (1–3 wt%)

Catalyst	S_{BET} ($m^2\ g^{-1}$)	S_n ($m^2\ g^{-1}$)	V_P (ml g^{-1})	PY (μmol m^{-2})		DMPY (μmol m^{-2})	
				473 K	573 K	473 K	573 K
APAl–P–0	136	144	0.50	0.60	0.12	0.06	—[a]
APAl–P–1S	120	116	0.50	0.63	0.21	0.11	—[a]
APAl–P–2S	111	110	0.50	0.92	0.22	0.13	—[a]
APAl–P–2.5S	103	105	0.49	1.00	0.34	0.14	—[a]
APAl–P–3S	120	123	0.47	0.89	0.28	0.13	—[a]
APAl–P–1F	138	148	0.60	0.49	0.21	0.15	—[a]
APAl–P–2F	85	88	0.41	0.76	0.29	0.25	—[a]
APAl–P–2.5F	47	52	0.36	1.38	0.55	0.43	0.09
APAl–P–3F	73	72	0.42	0.88	0.43	0.26	—[a]
APAl–P–0M	225	232	0.63	0.49	0.31	0.11	—[a]
APAl–P–2.5FM	79	81	0.42	1.01	1.83	0.59	0.18

[a] Not measured.

the acidity is still an open question since the structure of surface sulfate species depend on the nature of the metal oxide (7, 8, 38–41). Thus, bridged bi- and tridentate sulfate species have been claimed as the most probable ones.

Moreover, the DRIFT spectra (Figs. 5b–5d) of a less hydroxylated surface, like $AlPO_4$ (AP–A) obtained in aqueous ammonia and loaded with high amounts (1–10 wt%) of sulfate ions (15), showed an intense band at 1405 cm^{-1}, assigned to the asymmetric vibration of S=O bonds of $O_2S(O-)_2$ species, as well as bands at $\simeq$1000 and $\simeq$917 cm^{-1} mainly from the S–O vibrations of the $S(O-)_2$ group. The band at 1405 cm^{-1} increased in intensity as sulfate loading increased.

Thus, it clearly appears that sulfate species can be formed by impregnation of APAl–P (or AP–A) by $(NH_4)_2SO_4$ and, therefore, the Lewis acid strength of the metal becomes stronger by the inductive effect of S=O in that complex.

Surface Acidity Measurements

Gas-chromatographic pulse techniques can provide acidity information at catalytic reaction temperatures (42). However, are unable to distinguish Brønsted and Lewis sites unless specific basic probes were used. Thus, it is known that DMPY is selectively adsorbed on Brønsted acid sites, but not on Lewis acid sites, because of a steric hindrance of two methyl groups, whereas sterically nonhindered PY is adsorbed on both Brønsted and Lewis acid sites (43, 44). The difference between PY and DMPY adsorption is a measure of the Lewis acid sites.

The distribution of acid sites (Lewis and Brønsted) in the APAl–P–F and APAl–P–S catalysts is given in Table 2 as the amount of PY and DMPY adsorbed at saturation at the given temperature.

As can be seen from Table 2, the number of strong acid sites (Brønsted and Lewis) increases with anion loading as compared to pure APAl–P–0 catalyst, independently of the ion type. Moreover, fluoridation slightly reduces the total number of acid sites; the number of sites which adsorb PY are essentially the same for all APAl–P–F catalysts. However, as the surface area strongly decreases due to fluorination, the number of acid sites per unit area sharply increases from pure APAl–P–0 to APAl–P–F catalysts. Thus, a maximum in the density of strong acid sites (at 573 K vs PY) is found for a 2.5 wt% F^-. The same occurs on DMPY adsorption. The APAl–P–2.5F catalyst exhibits the highest density of Brønsted acid sites which ought to make this catalyst the most active catalytically, as actually does happen (see below).

On the other hand, fluoride ion incorporation from a methanolic solution of ammonium sulfate develops a catalyst that exhibits higher surface acidity as well as acid density than the corresponding catalyst obtained by impregnation in aqueous solution exclusively.

Surface acidity measurements at 298 K and in liquid phase (results not shown), using a spectrophotometric method, lead to similar results. The results of such a study also show that APAl–P–0 catalyst has basic sites (measured vs benzoic acid and phenol) but these are removed by anion modification (45). Moreover, while SO_4^{2-} ion decreases slightly the number of surface basic sites, the F^- ion sharply decreases the surface basicity, more strongly as basic strength increases. Thus, APAl–P–F catalysts possessed almost exclusively surface acid characteristics, while sulfated APAl–P catalysts exhibit a surface acid-base character.

In summary, the introduction of F^- ions onto APAl–P

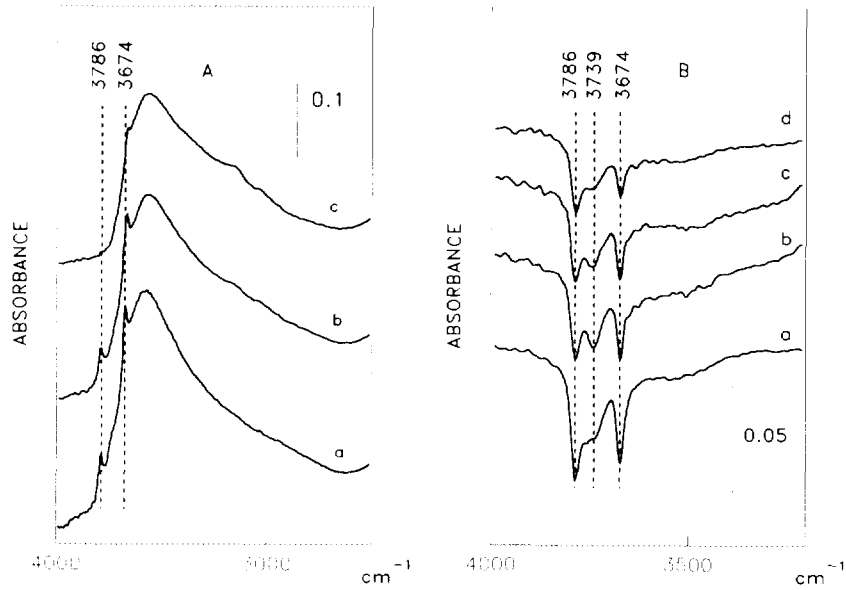

FIG. 4. DRIFT spectra (4000–2500 cm^{-1}). (A): (a) APAl–P–0, (b) APAl–P–2.5S, and (c) APAl–P–2.5F. (B): DRIFT spectra showing negative peaks due to OH removal on fluoridation of APAl–P catalyst (spectrum recorded at 573 K in the nitrogen stream). Reflectance spectra of APAl–P–F were ratioed automatically against the pure APAl–P background: (a) APAl–P–2.5FM, (b) APAl–P–3F, (c) APAl–25F, and (d) APAl–P–1F. All spectra were displaced for presentation.

catalyst results especially in an increase in the number of Brønsted acid sites of the highest strength (those that chemisorbed DMPY at 573 or 673 K) also increasing their surface density. So, these catalysts also exhibited hydrogen transfer processes in cyclohexene conversion (see below) unlike sulfate-treated ones.

DRIFT Measurements of PY and DMPY Adsorption

In order to prove the Brønsted nature of the acid sites, DRIFT spectroscopy of PY and DMPY adsorption (in atmosphere and temperature controlled *in situ* cell) was followed at various temperatures.

PY adsorption at 373 K followed by desorption at the same temperature (Fig. 6) gives rise to pyridinium cations, produced by the reaction of PY with surface Brønsted acid sites (bands at 1544 and 1636 cm^{-1}) and to species coordinated to Lewis acid sites (bands at 1451, 1493 and 1617 cm^{-1}) (46–48). The band at 1493 cm^{-1} can be attributed to PY chemisorption on one or the other or both Brønsted and Lewis sites. Besides, fluoride incorporation developed higher number of Brønsted acid sites as compared to sulfate impregnation.

Moreover, the desorption of PY a increasing temperatures results in the removal of both Brønsted-bound (1544 cm^{-1}) and Lewis-bound (1451 cm^{-1}) PY. However, Lewis-bound PY decreases significantly faster than the Brønsted-bound PY. At 573 K Brønsted-bound PY remained also evident on APAl–P–F catalysts but not on APAl–P–0 and APAl–P–S catalysts.

The development of Brønsted acidity by F^- ion is also strengthened by DMPY adsorption through the presence of a band at $\simeq$1636 cm^{-1} (Fig. 7) that is attributed to the vibration of 2,6-dimethylpyridinum ions ($DMPY^+$) (43, 44, 49).

Moreover, on the APAl–P–0 catalyst the $DMPY^+$ band was easily removed (results not shown) and thus completely vanishes on treatment in nitrogen at 473 K. However, on APAl–P–F catalysts some $DMPY^+$ band remained even at 573 K, showing that the number and strength of Brønsted acid sites are greater in fluorided samples than in the unloaded APAl–P catalyst.

Furthermore, since the area of the adsorption peak is proportional to the amounts of DMPY adsorbed, the changes in the peak area at $\simeq$1636 cm^{-1} (i.e., the Brønsted acidity) according to temperature were monitored for APAl–P–0 and APAl–P–F catalysts. In order to show the differences in these changes with fluoride loading clearly, the peak areas were normalized by the surface area (D_s) of every sample in the diffuse reflectance attachment, as shown in Fig. 8.

As can clearly be seen in Fig. 8, the normalized peak area (D_s) depends on the fluoride content of the APAl–P–F catalyst, showing a maximum (highest Brønsted acidity) at a fluoride loading of 2.5 wt%, a catalyst that shows the highest catalytic activity in cyclohexene and cumene conversions (see below). Note that the same behaviour is found in the variation of surface acid density (gas-chromatographically measured vs PY and

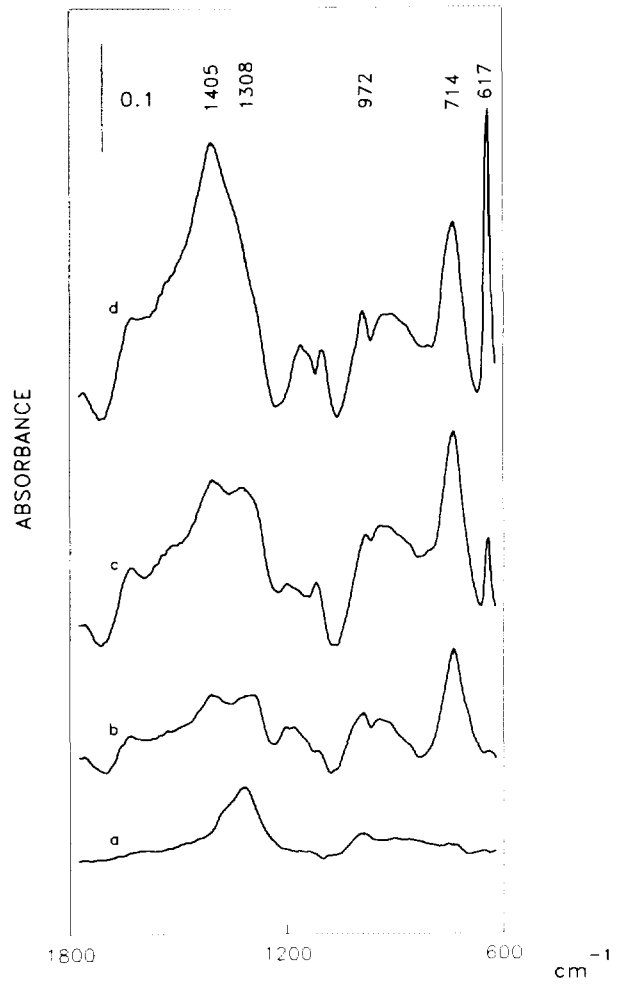

FIG. 5. DRIFT spectra (1800–600 cm^{-1}) of sulfated APAl–P and AP–A catalysts in the nitrogen stream (spectrum recorded at 573 K in the nitrogen stream): (a) APAl–P–3S, (b) AP–A–1S, (b) AP–A–3S, and AP–A–10S.

DMPY) of APAl–P–F catalysts as a function of anion loading (Fig. 9).

Catalytic Activity

In the absence of diffusional influences, the conversion (below 20%) of cyclohexene and cumene follows the requirements of Bassett–Habgood kinetic treatment (50) for first-order kinetic processes in which the rate determining step is the surface reaction,

$$\ln [1/(1 - X)] = RT\,kK\,(W/F),$$

where X is total conversion, k the rate constant of surface process, K the adsorption constant of the substrate on the catalyst, W the catalyst weight, and F the flow rate of carrier gas.

(a) *Cyclohexene Conversion*

Depending on the anion type, two categories of solids have to be considered. First, we have solids with SO_4^{2-} ions characterized by a tendency to promote skeletal isomerization almost exclusively, as occurs with $AlPO_4$ and pure APAl–P catalysts. In contrast, fluoride addition transformed a moderately active isomerization catalyst to one that shows high activity, exhibiting isomerization as well as hydrogen transfer activities which depended heavily on fluoride loading. Notwithstanding, the chief reaction is skeletal isomerization.

So, the main reactions that occur in cyclohexene transformation are: isomerization to 1- and 3-methylcyclopentene (1- and 3-MCPE; the 1-MCPE isomer always predominates) and hydrogen transfer with formation of methylcyclopentane (MCPA) and cyclohexane (CHA). Both MCPA and CHA involve bimolecular hydrogen transfer and all 5-ring products involve isomerization.

Other alkylated products such as dimethylcyclopen-

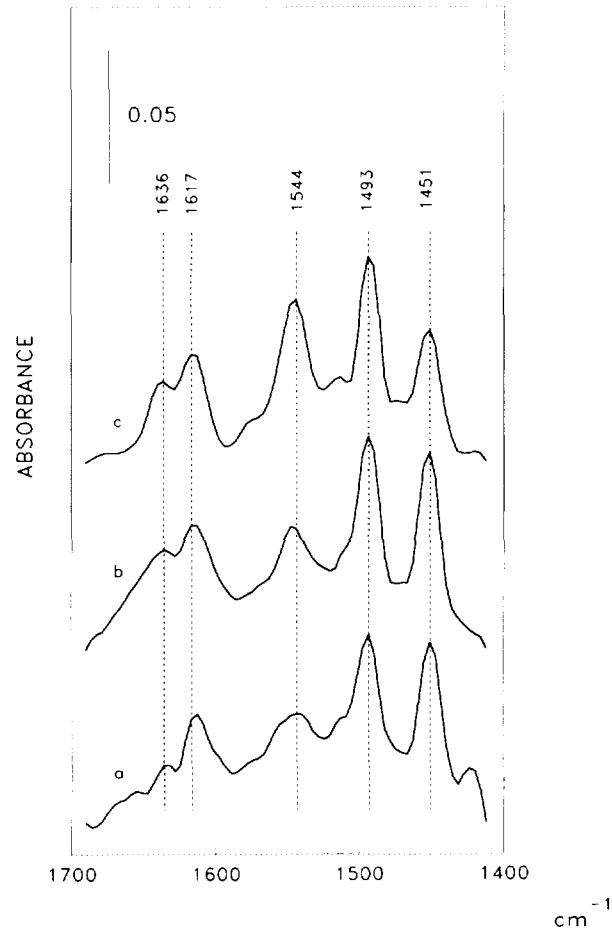

FIG. 6. DRIFT spectra of adsorbed PY (1700–1400 cm^{-1}: spectra of PY–APAl–P-0 (a), PY–APAl–P–2.5S (b), and PY–APAl–P–2.5F (c) which were treated at 373 K under nitrogen, after adsorption of PY, for 1 h.

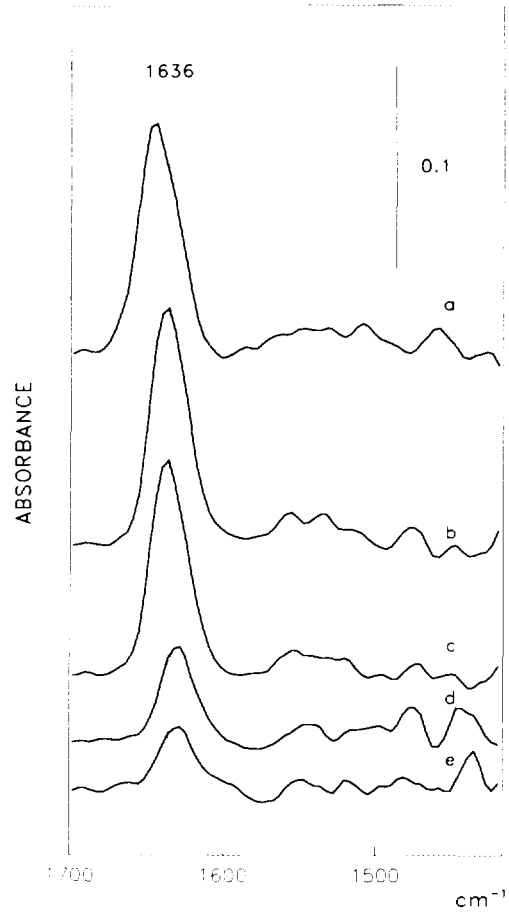

FIG. 7. DRIFT spectra of adsorbed DMPY (1700–1400 cm^{-1}): spectra of DMPY–APAl–P–3F which were treated at 373 K under nitrogen, after adsortion of DMPY, for 1 h (a). Then, the temperature was increased to 473 K and the catalyst remained, in the nitrogen stream, at 473 K additionally for 1 h (b); 3 h (c). Then, the temperature was increased to 573 K, the catalyst remaining at that temperature for 1 h (d); 3 h (e).

tane, dimethylcyclopentene, methylcyclohexane and methylcyclohexene, obtained in minor amounts on Y-zeolites (21) or SAPO-37 (21) were not observed in our experimental conditions (conversions below 20 mol%) over the most active catalysts (APAl–P–F). Benzene was not observed either. Only minor amounts of C_1–C_5 products result when high cyclohexene conversions (≈40 mol%) are obtained in order to develop useful OPE curves (see below).

Table 3 gives, for all the modified APAl–P catalysts, the apparent rate constants (kK_{SKI}), at a reaction temperature of 673 K) for skeletal isomerization from linear plots of ln $[(1/(1 - X_{SKI})]$ vs F^{-1}. Table 3 also includes activation parameters (E_a, ln A, $\Delta H^{\neq}$, $\Delta S^{\neq}$, and $\Delta G^{\neq}$), obtained through the Arrhenius and Eyring equations by plotting, respectively, ln kK_{SKI} vs T^{-1} and ln kK_{SKI}/T vs T^{-1}. Furthermore, in those cases where skeletal isomerization is

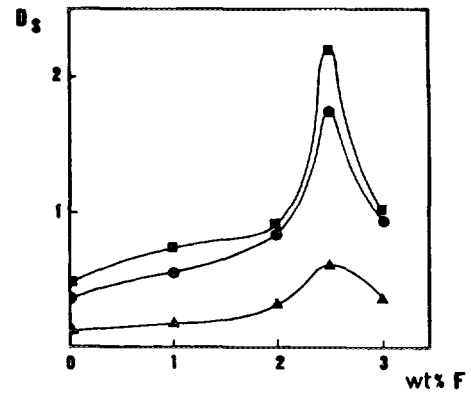

FIG. 8. Normalized $DMPY^+$ peak (=1636 cm^{-1}) area (D_s) in APAl–P–F catalysts as a function of anion loading: (■) 373 K, (●) 473 K, and (▲) 573 K.

the only reaction process, we also obtain kinetic selectivity factors (σ) with respect to 1-MCPE. σ values are also included in Table 3.

Table 4 gives, for all APAl–P–F catalysts, the apparent rate constants (kK_{HT}, at a reaction temperature of 673 K) as well as the activation parameters (E_a, ln A, $\Delta H^{\neq}$, $\Delta S^{\neq}$, and $\Delta G^{\neq}$) for hydrogen transfer process. Selectivities to hydrogen transfer (S_{HT}) are also included in Table 4.

A least-squares regression analysis shows, in all instances, correlation coefficients over 0.99. A t-test of significance, performed on the regression coefficients, show that these are significant at levels over 1%. At least three

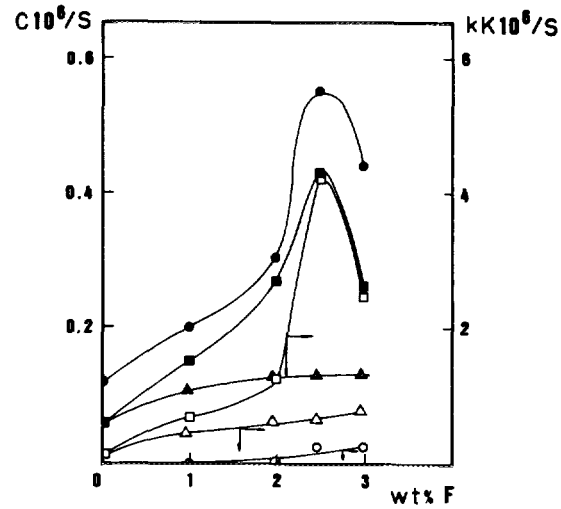

FIG. 9. Surface acid density (C/S) and specific catalytic activity (kK/S) as a function of anion loading: (●) acid density of APAl–P–F catalysts vs PY at 573 K; (■) acid density of APAl–P–F catalysts vs DMPY at 573K; (▲) acid density of APAl–P–S catalysts vs DMPY at 573 K; (□) kK_{SKI} per m^2 of APAl–P–F catalysts at 623 K; (○) kK_{HT} per m^2 of APAl–P–F catalysts at 623 K; (△) kK_{SKI} per m^2 of APAl–P–S catalysts at 623 K.

TABLE 3

Apparent Rate Constants at 623 K (kK_{SKI}), Activation Parameters (E_a, ln A, $\Delta H^{\neq}$, $\Delta S^{\neq}$, and $\Delta G^{\neq}$), and Selectivities to 1-MCPE (σ) for Cyclohexene Skeletal Isomerization on Unmodified and Anion-Treated $AlPO_4$–Al_2O_3 (25 wt% Al_2O_3) Catalysts

Catalyst	kK_{SKI} 10^6 (mol/atm m^2 s)	E_a (kcal/mol)	ln A^a	$\Delta H^{\neq}$ (kcal/mol)	$\Delta S^{\neq}$ (cal/mol K)	$\Delta G^{\neq b}$ (kcal/mol)	σ^c
APAl–P–0	0.12	12.8 ± 0.2	−0.7	11.5 ± 0.2	−63.1 ± 0.3	50.9 ± 0.3	1.9
APAl–P–0M	0.15	12.5 ± 0.5	−0.2	11.3 ± 0.4	−62.0 ± 0.6	50.0 ± 0.6	2.3
APAl–P–1S	0.46	12.1 ± 0.4	−0.1	10.9 ± 0.3	−61.7 ± 0.5	49.4 ± 0.5	2.4
APAl–P–2S	0.62	12.5 ± 0.4	0.5	11.2 ± 0.3	−60.7 ± 0.5	49.1 ± 0.5	2.6
APAl–P–2.5S	0.62	12.8 ± 0.7	0.6	11.6 ± 0.5	−60.5 ± 0.8	49.2 ± 0.7	2.8
APAl–P–3S	0.78	10.4 ± 0.5	−0.9	9.2 ± 0.5	−63.4 ± 0.5	48.7 ± 0.5	2.8
APAl–P–1F	0.68	16.8 ± 1.4	4.3	15.6 ± 0.7	−53.1 ± 1.2	48.7 ± 0.5	—[d]
APAl–P–2F	1.23	15.4 ± 1.0	3.3	14.3 ± 0.5	−55.1 ± 0.9	48.6 ± 0.7	—[d]
APAl–P–2.5F	4.20	14.1 ± 0.5	2.8	12.9 ± 0.4	−56.0 ± 0.7	47.8 ± 0.6	—[d]
APAl–P–3F	2.49	12.2 ± 0.8	1.2	11.0 ± 0.4	−59.1 ± 0.7	47.9 ± 0.6	—[d]
APAl–P–2.5FM	5.79	15.4 ± 1.1	4.8	14.3 ± 0.5	−52.0 ± 1.0	46.7 ± 0.9	—[d]

[a] A is expressed in mol/atm g s.
[b] At a reaction temperature of 623 K.
[c] Ratio of the fractional conversion of 1-MCPE to 3-MCPE (X_1/S_3).
[d] The catalyst also exhibits hydrogen transfer products (see Table 4).

measurements were used to calculate each kK. All values were reproducible to within about 8%.

As shown in Table 3, the activity of APAl–P catalyst in cyclohexene skeletal isomerization (SKI) is dramatically improved by anion loading. For APAl–P–S catalysts the activity gradually increased on increasing the amount of anion. Moreover, for APAl–P–F catalysts the activity gradually increased as the fluoride content increased to 2.5 wt%. When the fluoride content of the catalyst further increased to 3 wt%, a slight decrease in activity was observed for the whole temperature range studied. Furthermore, the activity of the catalyst increases by four-seven orders of magnitude on going from APAl–P–0 to APAl–P–3S. In contrast, APAl–P–F samples show activities which were in the range 6–40 times higher than that measured for the APAl–P–0 catalyst. The optimum in the apparent rate constant (kK_{SKI}) versus the amount of F^- ion can be attributed to a balance between two competitive effects, i.e., reduction of the number of Bronsted acid sites and the increase in their acid strength: as the fluoride content increases, the Bronsted acidity of the remaining surface hydroxyls must increase, but the number of such hydroxyls will decrease as they are replaced by fluorine (see above).

On the other hand, Table 4 shows the effect of various weight percentages of F^- ion on the apparent rate constants for hydrogen transfer reactions (kK_{HT}). As can be seen, HT is initially very weak (573 K) but then increases rapidly with an increase in reaction temperature regardless of fluoride loading. Moreover, HT selectivity increases with increasing fluoride content although SKI always predominates.

Notwithstanding, fluoride impregnation from a methanolic solution of ammonium fluoride leads to a catalyst that exhibits higher cyclohexene conversion with increased selectivity to HT reaction. This increase in activity is also found when comparing unmodified APAl–P catalysts: the catalyst treated with methanol/water exhibits higher catalytic activity than the catalyst treated with water exclusively. This is due to the smaller degree of modification of the support texture by treatment with methanol and, hence, is due to a lesser decrease in surface Brønsted acidity (see above).

So, in order to obtain highly active catalysts by fluoride loading, the impregnation ought to be carried out in that solvent which affects the porous texture of $AlPO_4$ support slightly. Therefore, it should be realized that not only the content of F^- ion, but also the use of methanol as an impregnating solvent is important for the preparation of highly active $AlPO_4$–Al_2O_3 catalysts for particular reactions.

Furthermore, HT reaction is also promoted in APAl–P–F catalysts where the Bronsted acid site density is a determining factor for bimolecular reactions such as HT. So, the presence of fluoride ion also increases the density of the Bronsted acid sites thus modifying the selectivity for HT in relation to pure APAl–P catalyst. Thus, the K_{HT}/K_{SKI} ratio increases as fluoride loading increases although in all APAl–P–F catalysts SKI is much faster than HT, about nine times for the most active catalyst (APAl–P–2.5FM).

So, in cyclohexene conversion, the activity of the catalysts is consistent with that of the surface density of acid sites measured by PY and DMPY adsorption (gas-chroma-

TABLE 4

Apparent Rate Constants at 623 K (kK_{HT}), Activation Parameters (E_a, ln A, $\Delta H^{\neq}$, $\Delta S^{\neq}$, and $\Delta G^{\neq}$), and Selectivities to HT (S_{HT}) for Hydrogen Transfer in Cyclohexene Conversion on Fluoride-Treated $AlPO_4$–Al_2O_3 (25 wt% Al_2O_3) Catalysts

	APAl-P-1F	APAl-P-2F	APAl-P-2.5F	APAl-P-3F	APAl-P-2.5FM
kK_{HT} 10^6 (mol/atm m^2 s)	0.02	0.08	0.26	0.24	0.64
ln A	1.6	1.4	1.4	1.8	1.9
E_a (kcal/mol)	17.8 ± 1.4	16.5 ± 0.7	15.8 ± 0.3	15.9 ± 0.8	20.9 ± 0.7
$\Delta H^{\neq}$ (kcal/mol)	16.5 ± 0.7	15.3 ± 0.4	14.6 ± 0.3	14.7 ± 0.5	19.8 ± 0.4
$\Delta S^{\neq}$ (cal/mol K)	−58.5 ± 1.2	−58.9 ± 0.7	−58.8 ± 0.5	−57.9 ± 0.9	−46.0 ± 1.0
$\Delta G^{\neq a}$ (kcal/mol)	53.0 ± 1.0	52.0 ± 0.6	51.2 ± 0.4	50.7 ± 0.8	48.4 ± 1.2
S_{HT} 523 K	2.6	5.0	4.5	5.4	10.3
573 K	2.8	5.5	5.2	7.4	13.2
623 K	3.2	6.2	6.2	10.0	16.7
673 K	3.8	7.4	7.6	13.7	21.3

[a] At a reaction temperature of 623 K.

tography and DRIFT measurements). The results suggest that the differences between the activities of various samples arise from the different Brønsted acidity of these catalysts. This is evident from Fig. 9 which represents the variation of surface acid density (C/S, vs PY and DMPY at 573 K) as well as the activity per square meter (kK/S) as a function of anion loading.

On the other hand, APAl–P–F catalysts were difficult to deactivate by coke deposition, maintaining stable activity.

Reaction network. For each reaction product, the optimum performance envelope (OPE) curve (51), which describe the selectivity behaviour of products, was obtained by plotting the fractional conversion of a particular product (X) against the total conversion (X_T), as illustrated in Fig. 10 for APAl–P–2.5S and APAl–P–2.5 FM catalysts.

We have plotted all the experimental data corresponding to different temperatures and contact times on the same diagram. Using such a procedure, an insignificant scattering of the data is evident on the selectivity diagrams and so clear tendencies can be observed from these curves.

Two behaviors have been established. On APAl–P–0 and APAl–P–S (Fig. 10A) catalysts (for which only SKI is found), 1- and 3-MCPE are stable primary competitive products coming from cyclohexene through a parallel process with a first-order kinetics (straight lines at origin in all cases). They are therefore formed at a constant rate in relation to feed conversion, and neither disappear nor accumulate due to secondary products. A primary product is defined as that which is produced from the reactant, no matter how many surface intermediates are involved in its formation.

For APAl–P–F catalysts, for which SKI is found together with HT, the situation changes (Fig. 10B). Now, 1- and 3-MCPE seem to be unstable primary competitive products coming from cyclohexene through a parallel process with first order kinetics since a downward deviation is found in their OPE curves. This downward deviation, which is so much more accentuated the more is the fluoride loading of the catalyst, is due to the formation of MCPA by HT. Thus, the OPE curve for MCPA corresponded to a stable secondary product since a zero slope at the origin, together with an upward deviation as X_T increases, is found by plotting its fractional conversion (X_{MCPA}) vs total conversion. It is formed by HT to MCPEs which are formed by the isomerization of cyclohexene and are capable of further reaction via bimolecular HT to give the secondary product MCPA. The yield of MCPA increases as the fluoride content of APAl–P–F catalyst increases. On the other hand, the yield of CHA (which is produced only over the most active catalysts and in a very low amount) as a function of cyclohexene conversion follows a straight line to the origin and so, CHA can be characterized as a primary stable product. This suggests that CHA is formed directly by HT to the reactant cyclohexene. Besides, its initial selectivity, given by the slope of the lines, remains almost unchanged (approaching zero) with the fluoride loading.

Contrary to SKI which is a unimolecular reaction and should occur on all sites, including the isolated ones, HT needs two neighbouring sites. To rationalize the bi-site character of HT, des Rochetes *et al.* (52) have proposed a reaction mechanism according to which a cycloalkene (cyclohexene or MCPE) molecule is maintained between a carbenium ion adsorbed on a first site and a neighbouring vacant acid site. Providing that the two sites are close enough, a hydride transfer could occur between the adsorbed cycloalkene molecule towards the carbenium ion.

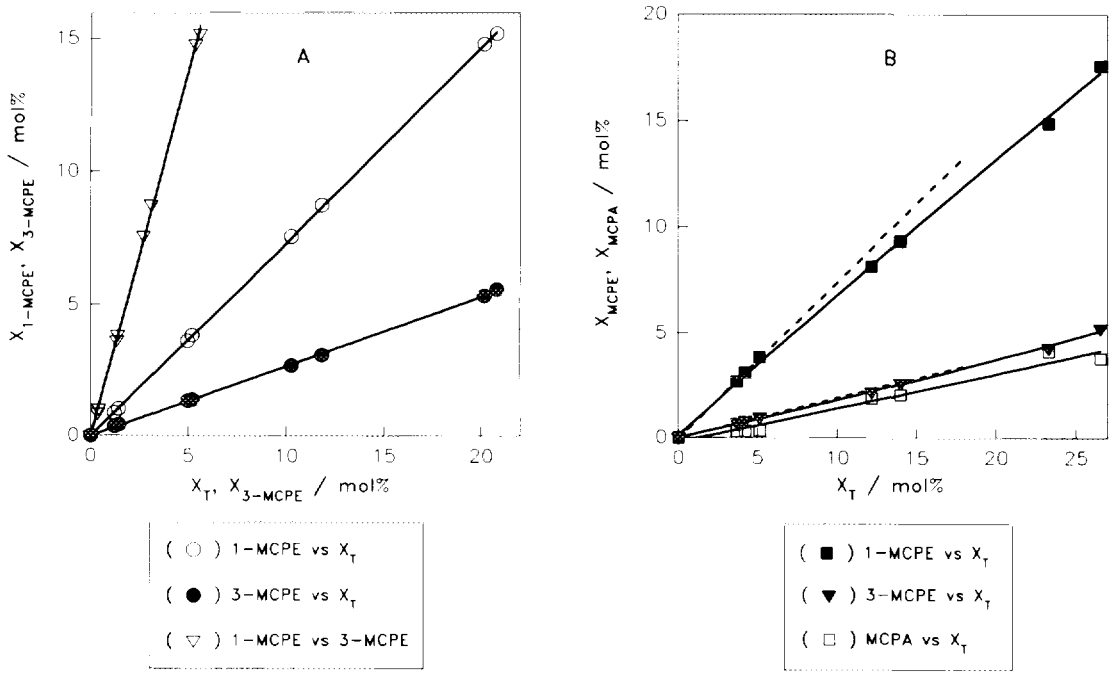

FIG. 10. (A) OPE curves [$X_{1\text{-MCPE}}$ and $X_{3\text{-MCPE}}$ vs X_T] and Wheeler selectivity [$X_{1\text{-MCPE}}$ vs $X_{3\text{-MCPE}}$] for cyclohexene skeletal isomerization on APAl–P–2.5S catalyst. (B) OPE curves [$X_{1\text{-MCPE}}$, $X_{3\text{-MCPE}}$, and X_{MCPA} vs X_T] for cyclohexene conversion on APAl–P–2.5FM catalyst.

Thus, the latter desorbs as cycloalkane (CHA or MCPA) and is replaced on the first site by the allylic carbocation which has just been formed.

Hence, the previously proposed mechanism for cyclohexene isomerization on $AlPO_4$ (AP) and $AlPO_4$–Al_2O_3 (APAl) (29) can also be applied to APAl–P–S catalysts but, however, the reaction intermediates ought to be of a higher carbocationic character than AP and unmodified APAl catalysts. Thus, as surface acidity increases, the more the carbocationic character of intermediates develops and the more the ratios of rates for 1- and 3-MCPE formation are expected to rise due to the higher stability of 1-methylcyclopentyl carbenium ion (II) in relation to 2-methylcyclopentyl carbenium ion (III). Besides, several studies (53, 54) proved that the cyclohexylcarbenium ion (I) rearranges spontaneously to the more stable 1-methylcycloentyl carbenium ion (II). Also, this tertiary 1-methylcyclopentyl ion was optimized and the energy is 15.2 kcal mol^{-1} below the 2-methylcyclopentyl ion.

Furthermore, to account for the results found with APAl–P–F catalysts, the mechanism exposed above ought to be enlarged in order to take into account the formation of HT products (Fig. 11).

Thus, the methylcyclopentyl carbenium ions (especially the II ion) and the cyclohexyl carbenium ion are intermediates for, respectively, the formation of MCPA and CHA. The greater stability of 1-methylcyclopentyl carbenium ion (II) in relation to the cyclohexyl carbenium ion lets us assume that most of the acid sites are occupied by such tertiary carbenium ions. This is supported by the greater production (almost exclusive) of MCPA as compared to CHA. This is also found by Magnoux *et al.* for cyclohexene conversion on ultrastable Y-zeolite catalysts (19).

(*b*) *Cumene Conversion*

Under the experimental conditions used, the dominant reaction is the cracking to produce propylene and benzene, which account 100 mol% for APAl–P–F catalysts. Dehydrogenation to α-methylstyrene is found on APAl–P–0 and APAl–P–S catalysts.

The fractional conversion of the reaction at all temperatures is calculated based on the molar fraction of the unreacted cumene in the product stream. Best and Wojciechowski (55) suggest that the total disappearance of cumene is not a good measure of the extent of the cracking reaction, since cumene disproportionation becomes significant at lower temperatures. However, we find no evidence of a diisopropylbenzene peak, even at the lowest temperature. Hence cumene disproportionation is not significant in our experiments. This is attributed to the low partial pressure of cumene in the reactor due to the dilution of cumene by the carrier gas. Besides, the short contact time of cumene on the catalyst in the reactor results in relatively small conversions and negligible

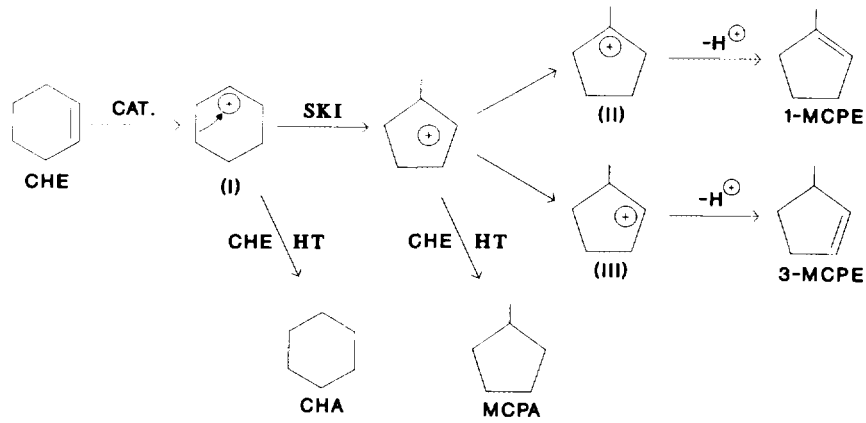

FIG. 11. Scheme of reaction for cyclohexene conversion on anion-treated APAl–P catalysts.

amounts of bimolecular reactions. We also see no evidence of *n*-propylbezene in the chromatograms, suggesting that the monomolecular reaction of isomerization of cumene may be negligible. So, under such conditions, it is reasonable to calculate the fractional conversion of the reaction based on the total disappearance of cumene.

Tables 5 and 6 set out the results of the apparent rate constants for cumene cracking (kK_{CK}) and cumene dehydrogenation (kK_{DH}), respectively, at a reaction temperature of 773 K. Tables 5 and 6 also include activation parameters (E_a, ln A, $\Delta H^{\neq}$, $\Delta S^{\neq}$, and $\Delta G^{\neq}$) obtained through the Arrhenius and Eyring equations.

As can be seen from Table 5, the catalytic activity of APAl–P–0 catalyst for cumene cracking was considerably increased by anion addition. Also, as in cyclohexene conversion, the fluoridation has been shown to play a major role in catalytic performance since it can better increase the conversion levels in cumene conversion (at least twelve orders of magnitude more active). Besides, F^- ion eliminates the formation of α-methylstyrene thus yielding selective catalysts for cracking. The importance of the fluoride-associated Brønsted acid sites becomes apparently on comparison of the cracking results for unmodified APAl–P catalyst. The cumene conversion is maximum at a loading of 2.5 wt% F^- and, furthermore, the solvent of impregnation exerts a remarkable effect on activity. Thus, the impregnation from a methanol/water solution of ammonium fluoride leads, as in cyclohexene conversion, to a catalyst that exhibits much higher cracking activity (about two times) that of the impregnated with an aqueous solution.

TABLE 5

Apparent Rate Constants at 773 K (kK_{CK}), Activation Parameters (E_a, ln A, $\Delta H^{\neq}$, $\Delta S^{\neq}$, and $\Delta G^{\neq}$), and Selectivities to Cracking (S_{CK}) for Cumene Cracking on Unmodified and Anion-Treated $AlPO_4$–Al_2O_3 (25 wt% Al_2O_3) Catalysts

Catalyst	kK_{CK} 10^7 (mol/atm m^2 s)	E_a (kcal/mol)	ln A^a	$\Delta H^{\neq}$ (kcal/mol)	$\Delta S^{\neq}$ (cal/mol K)	$\Delta G^{\neq b}$ (kcal/mol)	$S_{CK}{}^b$ (mol%)
APAl–P–0	0.04	22.4 ± 0.3	−0.1	20.8 ± 0.2	−62.2 ± 0.2	68.9 ± 0.3	63.3
APAl–P–0M	0.05	22.9 ± 0.3	1.2	21.3 ± 0.2	−59.7 ± 0.3	67.5 ± 0.3	79.5
APAl–P–1S	0.05	21.2 ± 0.6	−0.5	19.8 ± 0.4	−63.1 ± 0.5	68.5 ± 0.6	67.3
APAl–P–2S	0.08	18.5 ± 0.4	−1.8	17.1 ± 0.3	−65.7 ± 0.4	67.9 ± 0.4	85.3
APAl–P–2.5S	0.10	19.8 ± 0.6	−0.9	18.3 ± 0.4	−63.8 ± 0.5	67.6 ± 0.6	88.6
APAl–P–3S	0.18	20.2 ± 0.8	0.1	18.7 ± 0.5	−61.8 ± 0.8	66.5 ± 0.8	91.6
APAl–P–1F	0.45	22.2 ± 0.7	2.5	20.7 ± 0.4	−57.1 ± 0.5	64.9 ± 0.6	100[c]
APAl–P–2F	2.24	24.9 ± 0.6	5.4	23.5 ± 0.4	−51.3 ± 0.5	63.2 ± 0.6	100[c]
APAl–P–2.5F	7.09	22.8 ± 0.5	4.6	21.4 ± 0.3	−52.9 ± 0.5	62.3 ± 0.5	100[c]
APAl–P–3F	3.47	24.7 ± 0.6	5.5	23.2 ± 0.4	−51.1 ± 0.6	62.7 ± 0.6	100[c]
APAl–P–2.5FM	12.10	20.3 ± 0.3	4.0	18.9 ± 0.2	−54.0 ± 0.3	60.7 ± 0.3	100[c]

[a] A is expressed in mol/atm g s.
[b] At a rection temperature of 773 K.
[c] At all reaction temperatures (623–773 K).

TABLE 6

Apparent Rate Constants at 773 K (kK_{DH}) and Activation Parameters (E_a, ln A, $\Delta H^{\neq}$, $\Delta S^{\neq}$, and $\Delta G^{\neq}$) for Cumene Dehydrogenation on Unmodified and Anion-Treated $AlPO_4$–Al_2O_3 (25 wt% Al_2O_3) Catalysts

Catalyst	kK_{CK} 10^6 (mol/atm g s)	E_a (kcal/mol)	ln A^a	$\Delta H^{\neq}$ (kcal/mol)	$\Delta S^{\neq}$ (cal/mol K)	$\Delta G^{\neq b}$ (kcal/mol)
APAl–P–0	0.4	19.5 ± 0.6	−2.2	17.9 ± 0.6	−66.5 ± 0.5	69.3 ± 0.6
APAl–P–0M	0.5	12.5 ± 0.3	−6.4	11.1 ± 0.3	−74.7 ± 0.3	68.9 ± 0.4
APAl–P–1S	0.3	20.0 ± 0.5	−1.9	18.5 ± 0.5	−65.9 ± 0.5	69.2 ± 0.6
APAl–P–3S	0.4	14.2 ± 0.4	−5.6	12.7 ± 0.4	−73.1 ± 0.6	69.2 ± 0.6

[a] A is expressed in mol/atm g s.
[b] At a reaction temperature of 773 K.

These facts suggest that the enhancement of the cracking activity by the loading of F^- ions is related to the Brønsted acid properties of the site produced by the interaction of APAl–P and F^- ion. The increase in acid strength is confirmed by the fact that an increase in activity is more pronounced for cumene than for cyclohexene. Indeed, the slower the reaction the stronger the sites required for catalysis and, consequently, the more pronounced the effect on an increase in the acid strength. Thus, for the most active catalysts (2.5 wt% F^-) the impregnation in methanol generates fluoride-associated Brønsted acid sites whose strength is higher than those caused by impregnation in water: the increase in activity for cumene conversion is more than the increase in activity for cyclohexene conversion. Reactions of both hydrocarbons show similar trends for the catalysts studied. The activity drop over 2.5 wt% F is caused by a decrease in the density of the strongest Brønsted acid sites. In this sense, cumene cracking correlates better with strong acid sites determined by using DMPY than those determined by PY, as to be expected if this reaction occurs mainly on strong protonic sites. A *linear dependence* was obtained between *specific catalytic activity* (K_{CK} per m^2) and the *surface acid density* determined at 573 K by DMPY adsorption. This indicates that the ratio of catalytic and adsorption sites is constant, the centres are similar, and the mean productivity of a single site is constant.

For cumene conversion on APAl–P–S catalysts, the activity remained very low and the cracking selectivity (S_{CK}) varied with sulfate loading; S_{CK} increased with increasing reaction temperature and sulfate loading (Table 5). The maximum selectivity of cracking amounts to 63% (at 773 K) on the parent APAl–P catalyst and gradually increases with sulfate content reaching 92% for sample APAl–P–3S.

Furthermore, fluoride catalysts were difficult to deactivate by coke deposition from aromatic hydrocarbons maintaining a stable activity.

Reaction network. The Wheeler criterion (56) on the kinetic selectivity factor for first order processes and the OPE curves (51) indicates that (results not shown), in the range of conversions studied, both reaction products are stable primary products coming from cumene through a parallel process with first order kinetics.

Moreover, activities at different temperatures adjust to the same Wheeler's plot and E_a are virtually identical for all catalysts studied. These, together with the first order kinetics obtained, indicate that in all modified APAl-P catalysts the reaction proceeds on catalytic centres of the same kind and hence, the transition state is of the same type for all catalysts. Thus, differences in catalytic activities can be attributed to the more or less developed carbocationic character of the reaction intermediates which is a function of the acid strength of the catalyst.

Also, the negative values of $\Delta S^{\neq}$ indicate that, on going from the ground state to the transition state, there is a considerable decrease in the number of degrees of freedom. This highly ordered transition state is consistent with a reaction mechanism in which the slowest step is the stabilization and immobilization of reactant molecules on active acid sites on the catalyst. Furthermore, in Table 5 it can also be seen that $\Delta G^{\neq}$ changes slightly with respect to the catalyst. Besides, the reaction is entropy controlled ($T\Delta S^{\neq} > \Delta H^{\neq}$).

On the other hand, under cumene conversion the principal reaction over pure and anion treated APAl–P catalysts is cracking to benzene. The first step in this reaction is protonation of the ring of cumene, at the point of attachment of the substituent, on Brønsted acid sites followed by cleavage of the ring-side chain bond to generate benzene and propylene, as is generally accepted for cumene cracking over acidic catalysts (22, 24). In the case of

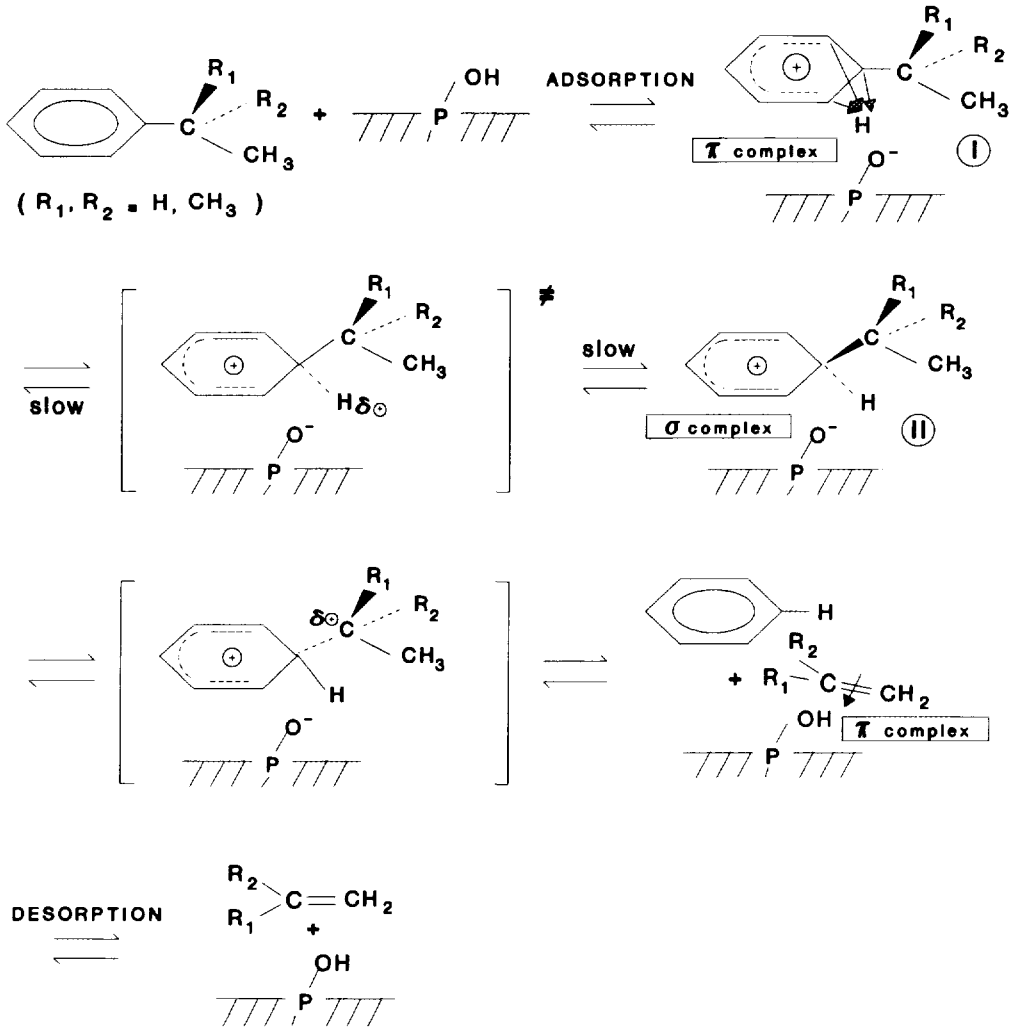

FIG. 12. Scheme of reaction for cumene conversion on anion-treated APAl–P catalysts.

$AlPO_4$ and related catalysts the reaction initiates through a π-complex (I), that involves the aromatic ring and the P–OH active site of the surface of the catalyst, as has been shown in previous works (57), applying the criteria of the frontier orbital theory (F.O.T.) to deduce the regioselectivity of the process. This intermediate progresses, in the slow step, towards a σ-complex (II) in which the ring-side chain has not left the ring. This would explain why the E_a values of the superficial process were approximately constant within the limits of experimental error. In subsequent rapid steps, the leaving of the ring-side chain would take place with the formation of the olefin (Fig. 12).

The importance of the fluoride-associate Brønsted acid sites becomes apparent on comparison of the cracking results for unmodified APAl–P–0 catalyst.

The formation of α-methylstyrene, in unmodified and sulfate-treated APAl–P catalysts, probably results from a free radical mechanism of cumene decomposition initiated by dehydrogenation centres (58).

CONCLUSIONS

It is concluded from this work that:

Modification of APAl–P catalyst with small amounts of F^- or SO_4^{2-} ions (1–3 wt%) considerably influences the surface properties. The most striking feature is the increase in surface acidity by ion loading. Thus, the introduction of F^- ions on APAl–P catalyst especially results in an increase in the number of Brønsted acid sites of the highest strength (which chemisorbed DMPY at 573 K). Besides, fluoridation has been shown to play a major role in the catalytic performance of APAl–P catalyst since it can better increase the conversion levels in cyclohexene as well as in cumene reactions as compared to sulfate-modified catalysts. Conversions of both hydrocarbons

show similar trends for the catalysts studied and correlated roughly with the change in acidity measured by DMPY adsorption. The positive effect of fluoride incorporation results from an increase in the density and strength of acid sites. This increase in acid strength is confirmed by the fact that the increase in activity is more pronounced for cumene than for cyclohexene. In that regard, the catalytic performances of APAl–P–2.5F are better than those of remaining fluorided catalysts. The initial activity is improved and the ratio of SKI activity to bimolecular HT activity for cyclohexene conversion decreases with increasing fluoride content. Also, APAl–P–F catalysts were 100% selective for the dealkylation of cumene to propylene and benzene. Furthermore, all APAl–P–F catalysts do not deactivate by coke deposition in the course of the catalytic processes.

Modification with sulfate anion leads to a smaller increase in acidity, and hence, in cyclohexene and cumene activity, than occurs with fluoride anion modification. Besides, only SKI is found in cyclohexene conversion, and cumene dehydrogenation competed with cumene cracking although the latter process always predominated.

ACKNOWLEDGMENTS

A.A.R. is indebted to the Consejería de Educación y Ciencia (Junta de Andalucía, España) for a doctoral fellowship. The authors acknowledge the subsidy received from the Dirección General de Investigación Científica y Técnica (DGICYT, Project PB89/0340), Ministerio de Educación y Ciencia, and from the Consejería de Educación y Ciencia (Junta de Andalucía), España. They also acknowledge the linguistic revision of the manuscript carried out by Professor M. Sullivan.

REFERENCES

1. Ghosh, A. K., and Kydd, R. A., *Catal. Rev. Sci. Eng.* **27,** 539 (1985), and references cited therein.
2. Matulewicz, E. R. A., Kerkhof, F. P. J. M., Moulijn, J. A., and Reitsma, H. K., *J. Colloid Interface Sci.* **77,** 110 (1980).
3. Kerkhof, F. P. J. M., Oudejans, J. C., Moulijn, J. A., and Matulewicz, E. R. A., *J. Colloid Interface Sci.* **77,** 120 (1980).
4. Allenger, V. M., Fairbridge, C., McLean D. D., and Ternan, *J. Catal.* **105,** 71 (1987).
5. Berteau, P., Kellens, M. A., and Delmon, B., *J. Chem Soc. Faraday Trans.* **87,** 1425 (1991).
6. Gerberich, H. R., Lutinski, F. E., and Hall, W. K., *J. Catal.* **8,** 286 (1967).
7. Saur, O., Bensitel, M., Saad, A. B. M., Lavalley, J. C., Tripp, C. P., and Morrow, B. A., *J. Catal.* **99,** 104 (1986).
8. Morrow, B. A., McFarlane, R. A., Lion, M., and Lavalley, J. C., *J. Catal.* **107,** 232 (1987).
9. Rayadhyaksha, R. A., and Chaudari, D. D., *Ind. Eng. Chem. Res.* **26,** 1743 (1987).
10. Hino, A., and Arata, K., *Mater. Chem. Phys.* **26,** 213 (1990), and references cited therein.
11. Sohn, J. R., and Jang, H. J., *J. Mol. Catal.* **64,** 349 (1991).
12. Waqif, M., Bachelier, J., Saur, O., and Lavalley, J. C., *J. Catal.* **72,** 127 (1992).
13. Campelo, J. M., Garcia, A., Luna, D., and Marinas, J. M., *J. Catal.* **102,** 299 (1986).
14. Campelo, J. M., Garcia, A., Luna, D., and Marinas, J. M., *in* "Preparation of Catalysts IV" (B. Delmon, P. Grange, P. A., Jacobs, and G. Poncelet, Eds.), p. 199. Elsevier, Amsterdam, 1987.
15. Campelo, J. M., Garcia, A., Luna, D., and Marinas, J. M., *React. Kinet. Catal. Lett.* **39,** 61 (1989).
16. Campelo, J. M., Garcia, A., Luna, D., Marinas, J. M., and Martinez, M. I., *Mater., Chem. Phys.* **21,** 409 (1989).
17. Bautista, F. M., Campelo, J. M., Garcia, A., Luna, D., Marinas, J. M., and Romero, A. A., *Appl. Catal.*, in press.
18. Guisnet, M., *Acc. Chem. Res.* **23,** 392 (1990).
19. Magnoux, P., Gallet, A., and Guisnet, M., *Bull. Soc. Chim. Fr.*, 810 (1987).
20. Parmaliana, A., Iannibello, A., Frusteri, F., Tsiakaras, T., and Giordano, N., *in* "Catalysis 1987" (J. W. Ward, Ed.), p. 43. Elsevier, Amsterdam, 1988.
21. Dwyer, J., Karim, K., and Ojo, A. F., *J. Chem. Soc. Faraday. Trans.* **87,** 783 (1991).
22. Prater, C. D., and Lago, R. M., *Adv. Catal.* **8,** 293 (1956).
23. Corma, A., and Wojciechowski, B. W., *Catal. Rev.-Sci. Eng.* **24,** 1 (1982).
24. Jacobs, P. A., Leeman, H. E., and Uytterhoeven, J. B., *J. Catal.* **33,** 17 (1974).
25. Midoratos, C., and Barthomeuf, D., *J. Chem. Soc. Chem. Commun.*, 39 (1981).
26. Becker, A. K., and Kowalak, S., *in* "Recent Advances in Zeolite Science" (J. Klinowski and P. J. Barrie, Eds.), p. 123. Elsevier, Amsterdam, 1989.
27. Ghosh, A. K., and Curthoys, G., *J. Chem. Soc. Faraday Trans. I* **79,** 2569 (1983).
28. Campelo, J. M., Garcia, A., Luna, D., and Marinas, J. M., *J. Mater. Sci.* **25,** 2513 (1990).
29. Campelo, J. M., Garcia, A., Luna, D., Marinas, J. M., and Martinez, M. I., *Mater. Chem. Phys.* **21,** 409 (1989).
30. Campelo, J. M., Garcia, A., Luna, D., Gutierrez, J. M., and Marinas, J. M., *Can. J. Chem.* **61,** 2567 (1983).
31. Yang, S. M., Lee, M. J., and Wu, S. T., *J. Chin. Chem. Soc.* **34,** 99 (1987).
32. Lorenz, P., Finster, J., and Wendt, G., *J. Electron Spectrosc. Relat. Phenom.* **16,** 267 (1979).
33. Muller, D., Jahn, E., Ladwig, G., and Haubenreisser, U., *Chem. Phys. Lett.* **109,** 332 (1984).
34. Blackwell, C. S., and Paton, R. L., *J. Phys. Chem.* **88,** 6135 (1984).
35. Sing, K. S. W., Everett, D. H., Haul, R. A. W., Moscou, L., Pierotti, R. A., Rouquerol, J., and Siemieniewska, T., *Pure Appl. Chem.* **57,** 603 (1985).
36. Lecloux, A. J., *in* "Catalysis-Science and Technology", (J. R. Anderson and M. Boudart, Eds.), Vol. 2, p. 171. Springer-Verlag, Berlin, 1981.
37. Farmer, V. C., "The Infrared Spectra of Minerals." Butterworths, London, 1974.
38. Jin, T., Machida, M., Yamaguchi, T., and Tanabe, K., *Inorg. Chem.* **23,** 4396 (1984).
39. Bensitel, M., Waqif, M., Saur, O., and Lavalley, J. C., *J. Phys. Chem.* **93,** 6581 (1989).
40. Yamaguchi, T., *Appl. Catal.* **61,** 1 (1990), and references cited therein.
41. Kim, S. I., and Woo, S. I., *J. Catal.* **133,** 124 (1992).
42. Kiselev, A. V., and Yashin, Y. I., "Gas Adsorption Chromatography." Plenum, New York, 1989.
43. Benesi, H. A., *J. Catal.* **28,** 176 (1973).
44. Corma, A., Rodellas, C., and Fornes, V., *J. Catal.* **88,** 374 (1984).
45. Bautista, F. M., Campelo, J. M., Garcia, A., Luna, D., Marinas, J. M., and Romero, A. A., *React. Kinet. Catal. Lett.*, **49,** 183 (1993).
46. Parry, E. P., *J. Catal.* **2,** 371 (1963).

47. Basila, M. R., Kantner, T. B., and Rhee, K. H., *J. Phys. Chem.* **68,** 3197 (1964).
48. Corma, A., Rodellas, C., and Fornes, V., *J. Catal.* **88,** 374 (1984).
49. Jacobs, P. A., and Heylen, C. F., *J. Catal.* **34,** 267 (1973).
50. Bassett, D., and Habgood, H. W., *J. Phys. Chem.* **64,** 769 (1960).
51. Ko, A. N., and Wojciechowski, B. W., *Prog. React. Kinet.* **12,** 201 (1983).
52. des Rochettes, B., Marcilly, C., Gueguen, C., and Bousquet, J., *Appl. Catal.* **58,** 35 (1990).
53. Wesdemiotis, C., Wolfschutz, R., and Schwarz, H., *Tetrahedron* **36,** 275 (1980).
54. Viruela-Martin, P. M., Nebot, I., Viruela-Martin, R., and Planelles, J., *J. Chem. Soc. Perkin Trans. 2,* 49 (1986).
55. Best, D. A., and Wojciechowski, B. W., *J. Catal.* **47,** 11 (1977).
56. Wheeler, A., *Adv. Catal.* **3,** 520 (1951).
57. Deya, P. M., Costa, A., Sinisterra, J. V., and Marinas, J. M., *Can. J. Chem.* **60,** 35 (1982).
58. Shao, E. T., and McInnich, E., J., *J. Catal.* **4,** 586 (1965).